Mineralogy and Petrology (2023) 117:191–200
https://doi.org/10.1007/s00710-022-00804-z

RESEARCH

Khurayyimite $Ca_7Zn_4(Si_2O_7)_2(OH)_{10}·4H_2O$: a mineral with unusual loop-branched *sechser* single chains

Biljana Krüger[1] · Irina O. Galuskina[2] · Evgeny V. Galuskin[2] · Yevgeny Vapnik[3] · Mikhail N. Murashko[4]

Received: 23 September 2022 / Accepted: 23 November 2022 / Published online: 28 December 2022

Abstract

The new mineral khurayyimite $Ca_7Zn_4(Si_2O_7)_2(OH)_{10}·4H_2O$ occurs in colorless spherulitic aggregates in small cavities of altered spurrite marbles located in the northern part of the Siwaqa pyrometamorphic rock area, Central Jordan. It is a low-temperature, hydrothermal mineral and is formed at a temperature lower than 100 °C. Synchrotron single-crystal X-ray diffraction experiments have revealed that khurayyimite crystallizes in space group $P2_1/c$, with unit cell parameters $a = 11.2171(8)$, $b = 9.0897(5)$, $c = 14.0451(10)$ Å, $\beta = 113.297(8)°$, $V = 1315.28(17)$ Å^3 and $Z = 2$. The crystal structure of khurayyimite exhibits tetrahedral chains of periodicity 6. The sequence of SiO_4 and $ZnO_2(OH)_2$-tetrahedra along the chain is Si–Si-Zn. The neighboring SiO_4-tetrahedra of the corrugated chains are bridged by additional $ZnO_2(OH)_2$-tetrahedra to form 3-connected *dreier* rings. The chains can be addressed as loop-branched *sechser* single chains $\{\boldsymbol{lB}, 1^1{}_\infty\}[^6Zn_4Si_4O_{21}]$. The chains are linked by clusters of five CaO_6 and two CaO_7 polyhedra with additional OH groups and H_2O molecules in the coordination environment. Based on the connectedness and one-dimensional polymerisations of tetrahedra $(TO_4)^{n-}$, chains of khurayyimite belong to the same group as vlasovite $Na_2ZrSi_4O_{11}$, since they can be described with geometrical repeat unit ${}^cT_r = {}^2T_4\ {}^3T_4$ and topological repeat unit ${}^cV_r = {}^2V_2\ {}^3V_2$.

Keywords New mineral · Loop-branched *sechser* chains · *Dreier* rings · Topology

Introduction

Spurrite marbles of the Siwaqa area, a pyrometamorphic complex in Central Jordan, have anomalously high contents of Zn (Khoury et al. 2016; Sokol et al. 2017; Vapnik et al. 2019). Most common Zn-bearing minerals are sulphides, but Zn can be found in selenides and oxides, too. In the northern part of the Siwaqa region, the mineral tululite $Ca_{14}(Fe^{3+}, Al)(Al, Zn, Fe^{3+}, Si, P, Mn, Mg)_{15}O_{36}$, was found in medium-temperature (800 – 850 °C) combustion metamorphic (CM) rocks i.e. Zn-rich marbles with high Ca:Al ratio (Khoury et al. 2016). A natural equivalent of $CaZn_2(OH)_6·2H_2O$ (Stahl and Jacobs 1997), named qatranaite (Vapnik et al. 2019), was recently discovered in the same area. Qatranaite was found in a single outcrop within cuspidine veins cutting spurrite marbles. This mineral is a product of low-temperature (< 70 °C) alteration of pyrometamorphic rocks by hyper-alkaline solutions (Vapnik et al. 2019). Furthermore, the mineral clinohedrite $CaZn(SiO_4)·H_2O$ was reported to replace sphalerite in the bleaching zones cutting through dark spurrite marbles from the same type locality (Khoury et al. 2016).

In the same area, we have found the new low-temperature hydrothermal mineral khurayyimite (IMA 2018–140), with ideal chemical formula $Ca_7Zn_4(Si_2O_7)_2(OH)_{10}·4H_2O$. To the best of our knowledge, no synthetic analogue is known and therefore, it is a new compound in the system CaO-ZnO-SiO_2-H_2O. The name khurayyimite is given after Mount Khurayyim (Jabal al Khurayyim), Siwaqa pyrometamorphic rock area, central Jordan. Khurayyimite was found in the immediate vicinity of this mountain. Type material was deposited in the mineralogical collection

Editorial handling: G. Giester

✉ Biljana Krüger
biljana.krueger@uibk.ac.at

[1] Institute of Mineralogy and Petrography, University of Innsbruck, Innrain 52, 6020 Innsbruck, Austria

[2] Faculty of Natural Sciences, Institute of Earth Sciences, University of Silesia, Będzińska 60, 41-200 Sosnowiec, Poland

[3] Department of Geological and Environmental Sciences, Ben-Gurion University of the Negev, POB 653, 84105 Beer-Sheva, Israel

[4] Faculty of Geology, Saint Petersburg State University, Universitetskaya Nab. 7/9, 199034 St. Petersburg, Russia

of the Fersman Mineralogical Museum, Leninskiy pr., 18/k2, 115162 Moscow, Russia, catalogue number: 5298/1.

Occurrence and genesis

The mineral khurayyimite, $Ca_7Zn_4(Si_2O_7)_2(OH)_{10}{\cdot}4H_2O$, occurs in small cavities and veins in altered spurrite marbles together with calcite, ettringite-thaumasite series minerals, Ca-hydrosilicates like jennite, $Ca_9(Si_3O_9)_2(OH)_6{\cdot}8H_2O$ and foshagite, $Ca_4(SiO_3)_3(OH)_2$ along with minerals of the tobermorite group. The type locality (N31°24.23′; E36°15.06′) is in Central Jordan, in the northern part of the Siwaqa pyrometamorphic rock area, circa 80 km south of Amman. Daba-Siwaqa is the largest area of the Hatrurim Complex (Mottled Zone) within the Dead Sea rift region, which exhibits twenty fields of pyrometamorphic rocks (Geller et al. 2012; Novikov et al. 2013).

Rock-forming minerals of unaltered dark spurrite marbles are spurrite $Ca_5(SiO_4)_2(CO_3)$, calcite $CaCO_3$, fluorapatite $Ca_5(PO_4)_3F$ and cuspidine $Ca_4Si_2O_7(F,OH)_2$. Accessory minerals spinel $MgAl_2O_4$—magnesioferrite $MgFe^{3+}{}_2O_4$, franklinite $ZnFe^{3+}{}_2O_4$, fluormayenite $Ca_{12}Al_{14}O_{32}[\square_4F_2]$—fluorkyuygenite $Ca_{12}Al_{14}O_{32}[(H_2O)_4F_2]$, sphalerite (Zn,Fe)S, pyrite FeS_2, chalcocite Cu_2S, hematite Fe_2O_3, clinohedrite $CaZn(SiO_4){\cdot}H_2O$. Furthermore, barite $BaSO_4$, celestine $SrSO_4$, selenides of Ni, Fe and Cu, greenockite CdS, elbrusite $Ca_3(Zr_{1.5}U^{6+}{}_{0.5})Fe^{3+}{}_3O_{12}$, perovskite $CaTiO_3$ and vorlanite $(CaU^{6+})O_4$ can be found (Galuskin et al. 2011a).

The formation of low-temperature zinc-bearing hydrated minerals in spurrite rock of the Hatrurim Complex was discussed in detail by Vapnik et al. (2019) in a publication on the mineral qatranaite, $CaZn_2(OH)_6(H_2O)_2$. The authors describe dark and fractured spurrite rocks, where cm-sized white zones are visible along the cracks. Within these zones re-crystallization of fine-grained spurrite, occurrence of metacrysts (up to 0.5 cm in size), and local enrichments in cuspidine are observed. The occurrence of qatranaite is restricted to cuspidine zones, whereas clinohedrite and khurayyimite are associated with the hydrated fragments of re-crystallized spurrite rock. Sphalerite is a widespread mineral in spurrite rock and it is considered to be a source of the zinc for the low-temperature minerals (Khoury et al. 2016). The stability of thaumasite (Jallad et al. 2003; Matschei and Glasser 2015) indicates that qatranaite, khurayyimite and clinohedrite are formed from highly alkaline solutions at ~70 °C, after the crystallization of thaumasite and calcite veins (Vapnik et al. 2019).

Results

Physical and optical properties

Khurayyimite forms colorless spherulitic aggregates up to 200–300 µm in size (Figs. 1, 2). Individual elongated platy

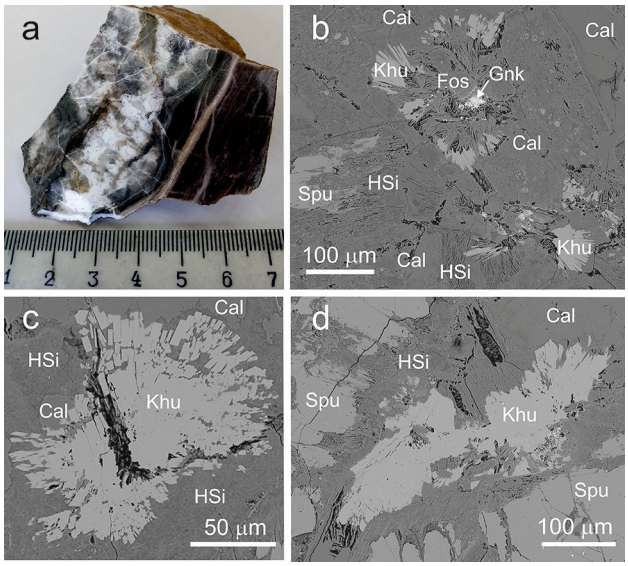

Fig. 1 Khurayyimite and associated minerals: **a** holotype specimen, contact of unaltered spurrite marble (brown) and altered spurrite marble (light), mainly composed of calcite, minerals of the ettringite-thaumasite series, Ca-hydrosilicates containing cavities with khurayyimite; **b**, **c** and **d** BSE images of typical spherulitic aggregates of khurayyimite: Cal—calcite, Fos—foshagite, Gnk—greenockite, HSi—mixture of Ca-hydrosilicates, Khu—khurayyimite and Spu—spurrite

crystals in the spherules are nearly 50 µm long, 20 µm wide and up to 10 µm thick. Crystals show white streak and white vitreous lustre. The measured micro-indentation hardness of khurayyimite gave Vickers Hardness $VHN_{25} = 242$ (average of 13 measurement), range 220–264 kg/mm^2, which corresponds to a value of 3.5–4 on the Mohs scale. Cleavage or parting were not observed. Tenacity is brittle and fracture is splintery. Because of the small size of the crystals, the density could not be measured. Instead, we calculated the density on the basis of the empirical formula and unit cell volume, as refined from single-crystal X-ray diffraction data. The calculated density is 2.806 g·cm^{-3}. The mineral dissolves in 10% HCl. Khurayyimite is optically negative, $\alpha = 1.603(2)$, $\beta = 1.607(2)$, $\gamma = 1.610(2)$ (at $\lambda = 589$ nm), $2V_{meas.} = 50(10)$ ° and $2V_{calc.} = 40.9$°. Dispersion of the optical axes is very weak; the optical orientation is: Z = b, X^c = 20(5)°, and it is non-pleochroic. Gladstone-Dale's compatibility factor is superior (1-(KP/KC) = -0.012).

Chemical composition

Quantitative wavelength-dispersive electron-microprobe analyses of khurayyimite and the associated minerals were carried out using a CAMECA SX100 electron probe microanalyser. A beam diameter of 10 µm was used. A counting time for peaks was 30 s and 15 s for the background. Diopside and sphalerite were used as reference materials for the

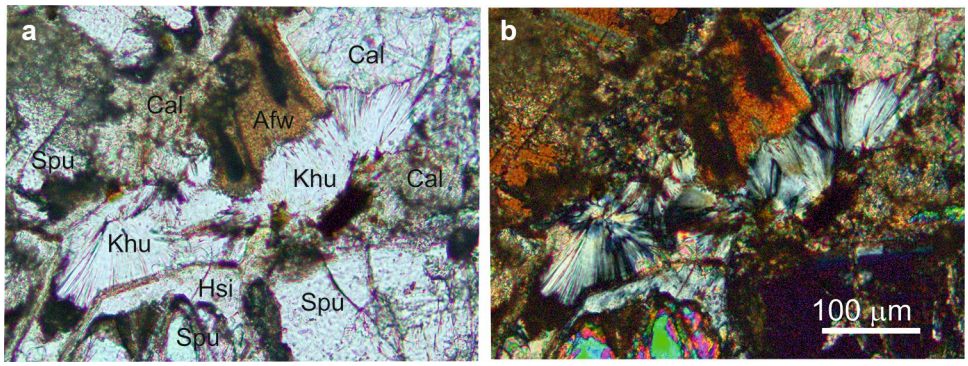

Fig. 2 Spherulitic aggregates of khurayyimite, from the same area as shown in Fig. 1d, presented in: **a** plane-polarized transmitted light and **b** cross-polarized transmitted light. Associated minerals are: Afw—afwillite with finely dispersed Fe hydroxides, Cal—calcite, HSi—mixture of Ca-hydrosilicates, Khu—khurayyimite and Spu—spurrite

analysis of Ca, Si and Zn (all *K*α lines). The holotype crystals of khurayyimite show uniform composition. The results based on eleven analyses are summed in the Table 1. The empirical formula, calculated on the basis of 28 O with $10(OH)^-$ and $4H_2O$ is $Ca_{7.070}Zn_{3.894}Si_{4.018}O_{14}(OH)_{10}·4H_2O$. The simplified and ideal formula is: $Ca_7Zn_4(Si_2O_7)_2(OH)_{10}·4H_2O$, which implies the following weight percentages: CaO 35.03, ZnO 29.05, SiO_2 21.45, H_2O 14.47. The total sum is quite low with ~96.28 wt%, because the measurement was done with a broad beam of 10 µm. Using a narrower beam the total wt% was higher, but the ratio of (Ca + Zn)/Si was worse. Because of the small size of the khurayyimite spherulites and difficulties to select pure material, H_2O and CO_2 contents were not determined by chemical methods. Moreover, absence of CO_3^{2-} groups and presence of H_2O and hydroxyl groups in khurayyimite were confirmed by the structural investigations and Raman spectroscopy.

X-ray crystallography

Single crystal diffraction experiments at ambient conditions were performed at the X06DA beamline of the Swiss Light Source (Paul Scherrer Institute, Villigen, Switzerland). The beamline was equipped with an Aerotech one-axis goniometer and a PILATUS 2 M detector.

Table 1 Chemical data for khurayyimite

Constituent	Mean wt%	Range wt%	Standard deviation (2σ)	Reference material
SiO_2	20.81	20.49–21.48	0.30	Diopside
ZnO	27.32	26.43–27.90	0.44	Sphalerite
CaO	34.17	33.66–34.54	0.24	Diopside
H_2O	13.98[a]			
Total	96.28*			

[a]calculated on the charge balance

*low sum, due the broad beam of 10 µm

Data collection was carried out at ambient conditions using the DA^+ acquisition software (Wojdyla et al. 2018). The radiation source was a SLS super-bending magnet (2.9 T). A wavelength of 0.70849 Å was obtained using a Bartels monochromator. The detector was placed 80 mm from the sample, resulting in a maximum resolution of 0.7 Å. A total of 1800 frames were recorded using fine-sliced (0.1°) ω-scans at 0.2 s per frame. Experimental details are given in Table 2.

Determination of lattice parameters, data reduction and absorption correction were processed with the program CrysAlisPro (Rigaku 2020). The average structure was solved using SIR2004 (Burla et al. 2005). The least-squares refinements were performed using the program Shelxl97 (Sheldrick 2008). Bond valence sum calculations were done with the BondStr program (Brown and Altermatt 1985; Rodríguez-Carvajal 2005). For the analysis of the chains in the structure of khurayyimite the Crystana software was employed (Klein and Liebau 2014). Figures of the crystal structure and deviations of the polyhedra from their ideal geometries expressed with the quadratic elongation *l* and the angle variance σ^2 as defined by (Robinson et al. 1971) were calculated using Vesta3 (Momma and Izumi 2011). All H-sites were located by difference Fourier analysis. The resulting structure model was refined using 223 parameters and 4676 independent reflections. All of the atoms, except H, were described using anisotropic displacement parameters. Hydrogen positions were refined at a fixed value of $U_{iso} = 0.05$ Å^2 for the H_2O molecules and OH groups bonded to cations. OH distances were constrained to 0.90(5) Å. Refinement details are summarized in Table 2. Table 3 lists atomic coordinates. In Table 4 selected bond distances, bond valence sums, quadratic elongation and bond angle variance are given. In the Table 5 parameters for H-bonds (D–A) are listed. A CIF is available in the Supplement.

As khurayyimite occurs only in tiny amounts X-ray powder diffraction data were not collected. Instead we calculated the powder pattern with Jana2006 (Petříček et al. 2014) using the structural data obtained from the single-crystal structure refinements. The seven strongest powder X-ray diffraction lines, *d* in Å (*I* %) *hkl* are: 3.8333 (100%) $\bar{2}13$; 10.3107 (81%)

Table 2 Parameters for X-ray data collection and crystal-structure refinement for khurayyimite

Crystal data	khurayyimite
Crystal system	monoclinic
Space group	$P2_1/c$ (no.14)
Unit cell dimensions	$a = 11.2171(8)$ Å $b = 9.0897(5)$ Å $c = 14.0451(10)$ Å $\beta = 113.297(8)°$
Volume	1315.28(17) Å^3
Z	2
Calculated density (g/cm^3)	2.829
Crystal size (mm^3)	0.04 × 0.02 × 0.01
Data collection	
Diffractometer	beamline X06DA, SLS
Detector, det. distance	PILATUS 2M, 80 mm
Exposure time (sec.) / step size (°)	0.2 / 0.1
Number of frames	1800
Max. θ range (°)	33.957
Index ranges	$-17 \le h \le 16$ $-14 \le k \le 13$ $-20 \le l \le 21$
No. of measured reflections	13,290
No. of unique reflections	4676
No. of obs. reflections (I > 2σ (I))	4336
Refinement	
no. of parameters	223
no. of restrained parameter	11
*R*int	0.0199
Rσ	0.0229
*R*1, I > 2σ(I)	0.0213
*R*1 all data	0.0230
*wR*2 on (F^2)	0.0689
GooF	1.092
Δρ min (e Å^{-3})	-0.60 close to Si2
Δρ max (e Å^{-3})	0.79 close to O13w

Table 3 Relative atomic coordinates and equivalent isotropic displacement parameters (Å^2)

Atom	*x/a*	*y/b*	*z/c*	U_{eq}*
Ca1	0.89144(3)	0.18921(3)	0.30782(2)	0.01276(6)
Ca2	0.67646(3)	0.50493(3)	0.30155(2)	0.01272(6)
Ca3	1.0000	0.5000	0.5000	0.01337(8)
Ca4	0.20729(3)	0.20321(3)	0.51355(2)	0.01191(6)
Zn1	0.63753(2)	0.15624(2)	0.40927(2)	0.01270(5)
Zn2	0.82709(2)	0.84331(2)	0.24413(2)	0.01251(5)
Si1	0.92362(4)	0.15302(4)	0.55974(3)	0.00902(8)
Si2	0.75247(4)	0.08831(5)	0.06319(3)	0.01059(8)
O1	0.87191(11)	0.21151(13)	0.11488(9)	0.0141(2)
O2	0.99086(11)	0.23555(13)	0.49134(9)	0.01261(19)
O3	0.74483(11)	0.01844(13)	0.16676(9)	0.0142(2)
O4	0.78829(11)	0.52816(13)	0.49012(9)	0.0130(2)
O5	0.97437(11)	0.94343(13)	0.34747(9)	0.0145(2)
O6	0.20015(11)	0.94589(13)	0.51133(9)	0.0145(2)
O7	0.62179(11)	0.32160(13)	0.49530(9)	0.0136(2)
O8	0.71327(12)	0.76094(14)	0.30632(9)	0.0157(2)
O9	0.67347(11)	0.24622(13)	0.29552(9)	0.0151(2)
O10	0.11959(12)	0.20571(14)	0.33439(9)	0.0151(2)
O11	0.88721(11)	0.45368(14)	0.31768(10)	0.0156(2)
O12	0.52523(11)	0.54754(14)	0.13247(9)	0.0163(2)
O13w	0.48487(13)	0.47597(19)	0.33205(12)	0.0264(3)
O14w	0.42763(14)	0.20105(17)	0.53742(14)	0.0275(3)
H8	0.6373(19)	0.802(4)	0.267(2)	0.050
H9	0.618(3)	0.211(3)	0.2357(15)	0.050
H10	0.143(3)	0.121(2)	0.317(3)	0.050
H11	0.925(3)	0.443(3)	0.2732(18)	0.050
H12	0.564(3)	0.590(4)	0.094(2)	0.050
H13B	0.523(3)	0.429(3)	0.3924(15)	0.050
H14A	0.484(3)	0.261(3)	0.525(3)	0.050
H13A	0.4105(19)	0.505(3)	0.335(3)	0.050
H14B	0.471(3)	0.124(3)	0.574(2)	0.050

*$U_{(eq)}$ is defined as one third of the trace of the orthogonalized U_{ij} tensor

100;214 2.9519 (68%) 031; 5.455 (59%) $\bar{1}21$; 2.6607 (57%) 114; 2.9084 (55%) $\bar{1}31$ and 3.4083 (42 %) $\bar{2}04$.

Crystal structure

The structure of khurayyimite exhibits dimers of SiO_4 tetrahedra, which are connected by $ZnO_2(OH_2)$-tetrahedra to form corrugated tetrahedral chains of periodicity six, extending along *b*. Each of the dimers Si_2O_7 of this *sechser* chain is bridged by another $Zn1O_2(OH)_2$-tetrahedron resulting in *dreier* rings of two Si- and one Zn-centered tetrahedra (Fig. 3a). According to the silicate nomenclature of Liebau (1985), these chains can be addressed as loop-branched *sechser* single chains $\{\boldsymbol{lB}, 1^1{}_\infty\}[^6Zn_4Si_4O_{21}](OH)_8$.

The chains are linking the clusters of seven CaO_n polyhedra made of two $Ca1O_7$ and five octahedra with Ca2, Ca3 and Ca4 atoms in the center (Fig. 3b and c). The clusters occur in two different orientations in the unit cell (Fig. 3d). The *sechser* chains are twisting around clusters sharing corners and edges with the CaO_n polyhedra. Three oxygen atoms shared by Zn-centered tetrahedra and CaO_n polyhedra are connected to additional H atoms (O8–H8, O9–H9, O10–H10 and O12–H12). Another hydrogen atom, H11 is attached to O11, an apical oxygen between Ca1-, Ca2- and Ca3-centered polyhedra (Fig. 3c). Ca2 is coordinated by one O anion, four OH^- groups and one H_2O molecule (H13A–O13w–H13B), where Ca4 is coordinated by three O anions, two OH^- groups and one H_2O molecule (H14A–O14w–H14B) (Fig. 3c,

Table 4 List of selected bond distances (Å) and bond valence sums (BVS, given in valence units) for cations in khurayyimite. Calculated quadratic elongation (l) and bond angle variance (σ^2 in $^{\circ 2}$) are quoted for all SiO_4/ZnO_4 tetrahedra and CaO_6 octahedra. In addition, volume ($Å^3$) is quoted for the tetrahedra

Ca1–O1	2.6387(14)	Ca2–O4	2.4504(12)	Ca3–O2×2	2.4070(12)	Ca4–O2	2.3406(13)
Ca1–O2	2.4065(12)	Ca2–O8	2.3597(13)	Ca3–O4×2	2.3374(13)	Ca4–O4	2.4432(12)
Ca1–O3	2.5420(11)	Ca2–O9	2.3529(12)	Ca3–O11×2	2.4026(13)	Ca4–O6	2.3401(12)
Ca1–O5	2.3993(12)	Ca2–O11	2.3309(14)			Ca4–O8	2.3490(12)
Ca1–O9	2.4377(14)	Ca2–O12	2.3411(11)			Ca4–O10	2.3113(12)
Ca1–O10	2.4404(14)	Ca2–O13w	2.3663(18)			Ca4–O14w	2.3592(17)
Ca1–O11	2.4095(13)						
Average	2.4677(5)	Average	2.3669(5)	Average	2.3823(5)	Average	2.3572(5)
BVS Ca1	1.960(3)	BVS Ca2	2.047(3)	BVS Ca3	1.960(3)	BVS Ca4	2.102(3)
l		*l*	1.0375	*l*	1.0291	*l*	1.0087
σ^2		σ^2	128.3211	σ^2	92.1824	σ^2	29.2968
Zn1–O6	1.9531(11)	Zn2–O3	1.9425(11)	Si1–O1	1.6757(14)	Si2–O1	1.6753(12)
Zn1–O7	1.9797(13)	Zn2–O5	1.9410(11)	Si1–O2	1.6210(15)	Si2–O3	1.6203(14)
Zn1–O9	1.9732(14)	Zn2–O8	1.9585(15)	Si1–O5	1.6115(11)	Si2–O4	1.6315(14)
Zn1–O12	1.9510(12)	Zn2–O10	1.9131(14)	Si1–O6	1.6236(11)	Si2–O7	1.6195(11)
Average	1.9642(6)	Average	1.9388(7)	Average	1.6329(6)	Average	1.6367(7)
V	3.83	V	3.67	V	2.22	V	2.23
BVS Zn1	1.981(3)	BVS Zn2	2.123(4)	BVS Si1	3.913(7)	BVS Si2	3.873(7)
l	1.0098	*l*	1.0118	*l*	1.0022	*l*	1.0058
σ^2	41.2545	σ^2	44.5173	σ^2	8.7905	σ^2	23.1684

Table 5). The chains extend infinitely along b. Along the a-direction the corrugation of the chains creates ~11 Å thick sheets (Fig. 3d, e). These sheets are interconnected by oxygen (O12) shared by $Ca2O_6$ polyhedra and $Zn1O_4$ tetrahedra (Fig. 4). In addition, the narrow gaps between the sheets, formed parallel to [001], are filled by strong hydrogen bonds formed between five OH^- groups two H_2O molecules attached to the chains or Ca-clusters.

The periodicity of crooked loop-branched *sechser* single chains $\{\boldsymbol{lB}, 1^1{}_\infty\}[^6Zn_4Si_4O_{21}](OH)_8$ along *b* is 9.0897 Å, which corresponds to the b lattice parameter of the cell. The stretching factor of the chain is rather small. Both SiO_4 tetrahedra within the chain show average bond lengths of 1.6329(6) and 1.6367(7) and low measures of distortion (Table 4). Two Zn-centered tetrahedra are equally distorted (see Table 4). Still $Zn1O_4$ has longer average bonds of 1.9642(6) Å than $Zn2O_4$ 1.9388(7). Actually, the larger $Zn1O_4$ tetrahedron forms a loop with the Si_2O_7 groups. Strong repulsive forces between the tetrahedra of the *dreier* ring are pressing O1 atom as far as possible forming a triangle with longer $Zn1O_4$ edge (~3.176 Å) and two shorter SiO_4 edges (2.66 and 2.68 Å). These repulsive forces are, according to Liebau (1985), a possible reason why such loops are only rarely observed.

Raman spectroscopy

The Raman spectrum of khurayyimite was recorded using a WITec alpha 300R confocal Raman microscope equipped with an air-cooled solid laser (488 nm) and a charge-coupled device detector operating at -61 °C. The laser radiation was coupled to a microscope through a single-mode optical fibre

Table 5 H-bond parameters

Donor (D) – H…Acceptor (A)	D – H (Å)	H…A (Å)	D…A (Å)	D—H…A (°)
O8–H8…O13w	0.89(3)	2.19(3)	3.020(2)	154(3)
O9–H9…O13w	0.88(2)	2.44(3)	3.144(2)	137(2)
O10–H10…O11	0.88(2)	2.34(3)	3.1124(18)	146(3)
O11–H11…O5	0.89(3)	2.38(3)	3.2632(18)	174(2)
O12–H12…O14w	0.90(3)	2.14(3)	2.986(2)	156(3)
O13w–H13A …O3	0.89(3)	1.74(3)	2.612(2)	166(3)
O13w–H13B…O7	0.89(2)	1.73(2)	2.608(2)	166(3)
O14w–H14A …O7	0.90(3)	1.84(4)	2.704(2)	160(3)
O14w–H14B…O12	0.90(3)	1.75(3)	2.633(2)	168(3)

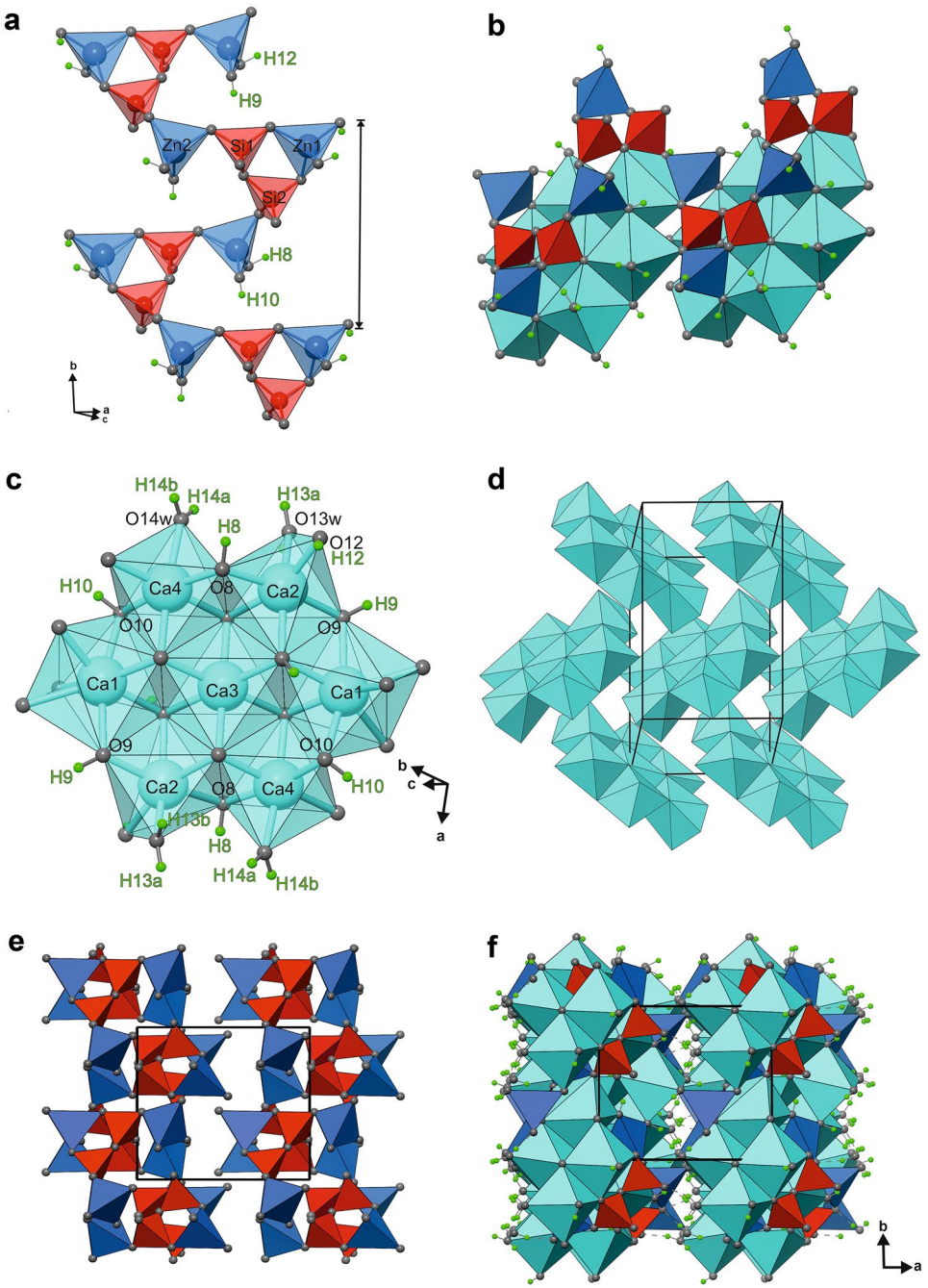

Fig. 3 The structure of khurayyimite: **a** loop-branched *sechser* single chains with *dreier* rings **b** single chain linking the two clusters of CaO_n polyhedra **c** clusters of CaO_n polyhedra with OH^- groups and H_2O molecules **d** different orientations of clusters in the unit cell **e** periodicity of crooked chain **f** crystal structure with chains, clusters and hydrogen bonds between them

with a diameter of 3.5 µm. An air Zeiss LD EC Epiplan-Neofluan DIC-100/0.75NA objective was used. Raman scattered light was focused on a broad band single mode fibre with effective Pinhole size about 30 µm and monochromator with a 600 mm^{-1} grating. The power of the laser at the sample position was ~30 mW. Integration times of 3 s with accumulation of 15 scans and a resolution 3 cm^{-1} were chosen. The monochromator was calibrated using the Raman scattering line of a silicon plate (Ntziouni et al. 2022). The following bands in the Raman spectra of khurayyimite, $Ca_7Zn_4(Si_2O_7)_2(OH)_{10}{\cdot}4H_2O$, were observed ($cm^{-1}$, Fig. 5): 80, 112, 143, 171, 203, 246, 270, 314, 342, 378, 436, 465, 524, 586, 676, 740, 821, 911, 916, 975, 1624, 2898, 3074, 3109, 3503, 3555, 3580, 3603, 3618, 3633.

The main bands correspond to Si-O vibrations in (Si_2O_7) 6-groups: ν1 911 cm^{-1}, ν4 676 cm^{-1}, ν2 378 cm^{-1} (Galuskin et al. 2011b) and Zn-O tetrahedra $ZnO_2(OH)_2$: ν1 465 cm^{-1}; ν2 + ν4 310cm^{1}, 314 cm^{-1}, 342 cm^{-1} (Lin et al. 1999; Kesic et al. 2014). The band at 586 cm^{-1} is related to SiO-Zn vibrations (Chandra Babu and Buddhudu 2014), and band at 524 cm^{-1} is related to Si-O-Si vibrations. The main bands below 203 cm^{-1} are due to vibrations of Ca-O in $CaO_4(OH)_3$ polyhedra

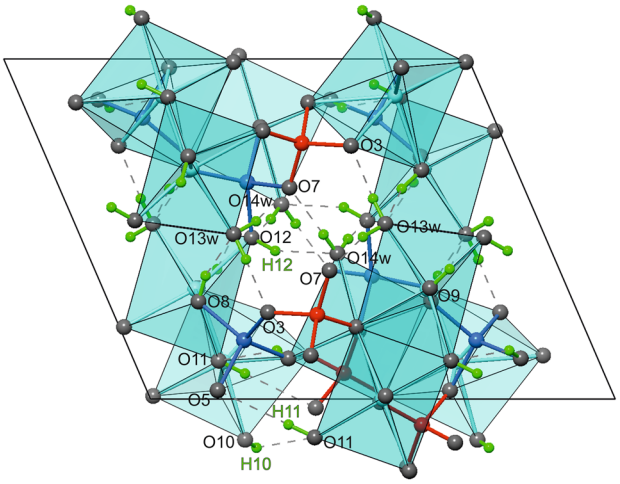

Fig. 4 The strong hydrogen bonds bridging CaO_n polyhedra and *sechser* chains

and $CaO(OH)_4(OH_2)$, $CaO_4(OH)_2$, $CaO_3(OH)_2(OH_2)$ octahedra. Bands at 2898, 3074 and 3109 cm^{-1} are related to O-H vibration in H_2O with strong hydrogen bonds, whereas the main bands at 3503, 3580, 3603 and 3618 cm^{-1} correspond to vibrations of OH groups.

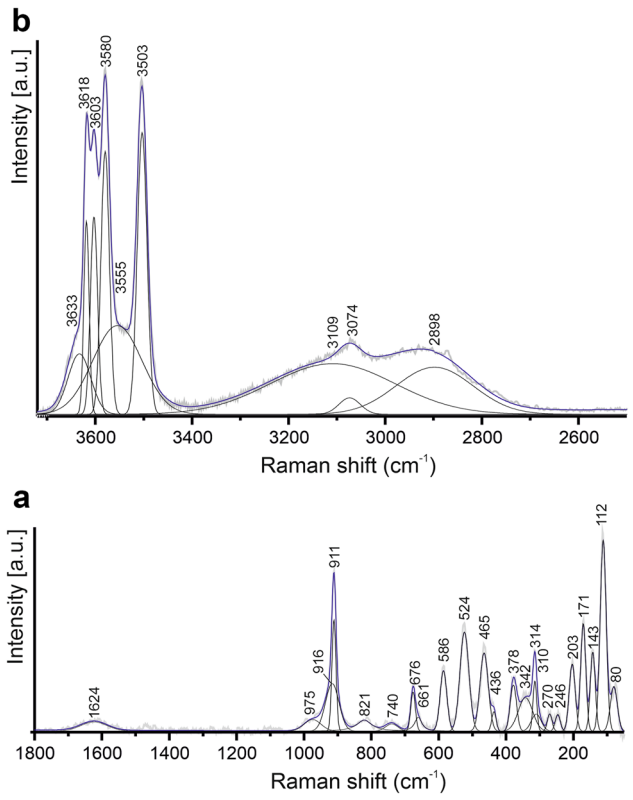

Fig. 5 Raman spectrum of khurayyimite: **a** in the region 1800–60 cm^{-1} **b** in the region 3800 2600 cm^{-1}

Discussion

The structure of this mineral comprises new and very unusual loop-branched *sechser* single chains that can be described with the formula $\{\boldsymbol{lB}, 1^1_\infty\}[^6Zn_4Si_4O_{21}](OH)_8$, following the classification of Liebau (1985). This formula denotes a loop-branched (***lB***) single chain (1^1_∞) with a six-tetrahedra repetition unit (*sechser*) made of four ZnO_4 and four SiO_4 corner-sharing tetrahedra ($Zn_4Si_4O_{21}$). In the chains, Si_2O_7 dimers and $ZnO_2(OH)_2$ tetrahedra are connected by corners building the loops i.e. *dreier* ring (Fig. 3a). This combination of the two SiO_4 and one ZnO_4 tetrahedra in a ring is very rare due to the strong repulsive forces in this formation. The volume of the ZnO_4 tetrahedra with ~3.97 $Å^3$ is two times larger than the volume of SiO_4 tetrahedra (~ 2.05 $Å^3$) (Abrahams and Bernstein 1969; Kato and Nukui 1976).

So far, only a few compounds are reported with the same ring formation but utterly different structures (see Fig. 6). One of them is a structure of synthetic $K_2ZnSi_2O_6$ (Hogrefe and Czank 1995), where two layers with three-membered rings ($2\times SiO_4$, $1\times ZnO_4$) are forming the loop-branched *zweier* framework $\{\boldsymbol{lB},^3_\infty\}[^2(Zn_1Si_2)O_6]$. In the structure of $K_2ZnSi_4O_{10}$ (Kohara and Kawahara 1990), a tectosilicate framework is built by ten-membered rings of SiO_4 tetrahedra interconnected with five-member rings ($4\times SiO_4$, $1\times ZnO_4$), four-membered rings ($3\times SiO_4$, $1\times ZnO_4$) and three-membered rings ($2\times SiO_4$, $1\times ZnO_4$).

Quite the contrary, three-membered rings comprising two ZnO_4 and one SiO_4 are widespread among zinc silicates, like in the minerals willemite Zn_2SiO_4 (Simonov et al. 1977), hemimorphite $Zn_4Si_2O_7(OH)_2·H_2O$ (Li and Bass 2020), hodgkinsonite $Zn_2MnSiO_4(OH)_2$ (Rentzeperis 1963), junitoite, $CaZn_2Si_2O_7·H_2O$ (Hamilton and Finney 1985), $K_2Zn_2Si_8O_{19}$ (Kohara and Kawahara 1990) etc.

Different combinations of chains and frameworks made of ZnO_4 and SiO_4 tetrahedra are known. In $ZnSiO_3$ (Morimoto et al. 1975), with Zn atoms in six- and four-fold coordination, two pyroxene-like chains are branched with two ZnO_4 tetrahedra forming four-member loops. The crystal structures of LT and HT forms $BaZn_2Si_2O_7$ (Lin et al. 1999) have a disilicate group Si_2O_7 linked via corners with ZnO_4 tetrahedra in a three-dimensional framework, which exhibits sixmember rings ($2\times Si_2O_7$, $2\times ZnO_4$), four member-rings ($2\times SiO_4$, $2\times ZnO_4$) and three-membered rings ($1\times SiO_4$, $2\times ZnO_4$).

Loop-branched *sechser* single chains are observed in vlasovite $Na_2ZrSi_4O_{11}$ (Sokolova et al. 2006; Voronkov and

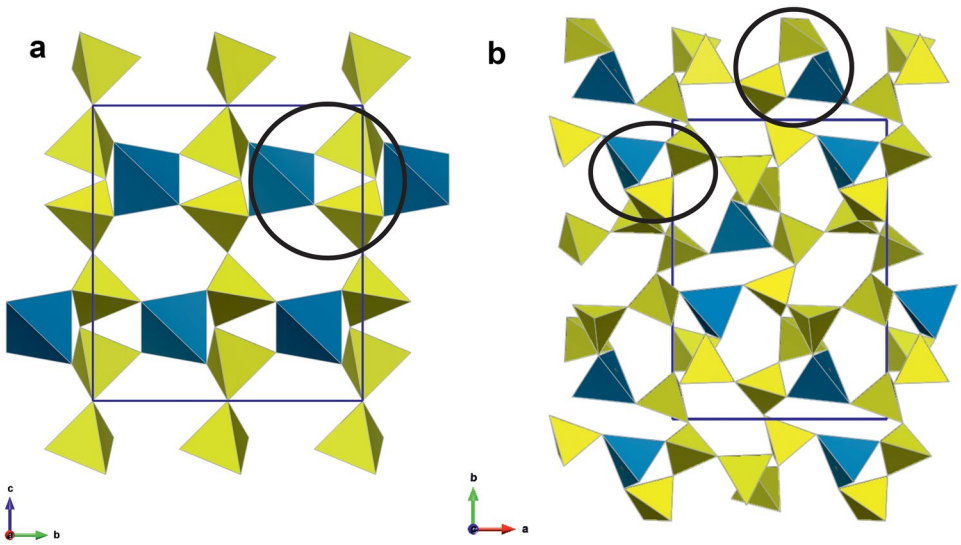

Fig. 6 *Dreier* rings in: **a** $K_2ZnSi_2O_6$ (Hogrefe and Czank 1995) and **b** $K_2ZnSi_4O_{10}$ (Kohara and Kawahara 1990). SiO_4 tetrahedra are shown in yellow and ZnO_4 in blue. K atoms were omitted for clarity

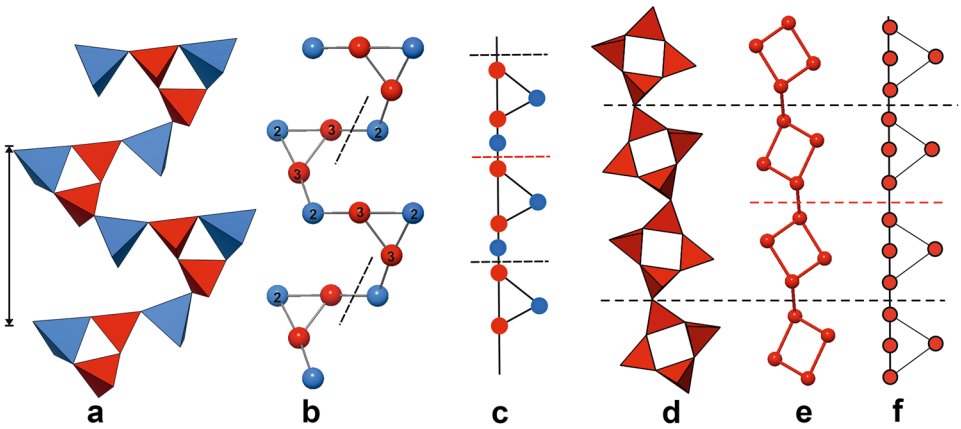

Fig. 7 **a** Khurayyimite chain $[Zn_4Si_4O_{21}]$ **b** khurayyimite geometrical repeat unit $n_g=6$ ${}^cT_r={}^2T_4\ {}^3T_4$ **c** khurayyimite topological repeat unit ${}^cV_r={}^2V_2\ {}^3V_2$ **d** vlasovite chain $[Si_8O_{22}]$ **e** vlasovite geometrical repeat unit $n_g=6$ ${}^cT_r={}^2T_4\ {}^3T_4$ **f** vlasovite topological repeat unit ${}^cV_r={}^2V_2\ {}^3V_2$

Pyatenko 1962). However, chains of vlasovite $\{\boldsymbol{lB}, 1^1_\infty\}$ $[{}^6Si_4O_{22}]$ exhibit four-membered rings of SiO_4-tetrahedra linked to form a chain (Liebau 1985). According to the structural hierarchy for chain, ribbon and tube silicates established by Day and Hawthorne (2020), khurayyimite has the same geometrical repeat unit ${}^cT_r={}^2T_4\ {}^3T_4$ and topological repeat unit ${}^cV_r={}^2V_2\ {}^3V_2$ as the mineral vlasovite and the three synthetic compounds $HNb(H_2O)[Si_4O_{11}](H_2O)$, $Cs_{0.66}H_{0.33}Nb(H_2O)[Si_4O_{11}]$ and $Na_2H(NbO)[Si_4O_{11}](H_2O)_{1.25}$ reported by Salvadó et al. (2001), and therefore they belong to the same group. This new structural hierarchy is based on the connectedness of one-dimensional polymerization of the $(TO_4)^{n-}$ tetrahedra.

The geometrical repeat unit has $n_g=6$ tetrahedra. Its connectivity is denoted as ${}^cT_r={}^2T_4\ {}^3T_4$; i.e. contains four ZnO_4 tetrahedra with connectivity of two ($^2T_4$) and four SiO_4 tetrahedra with connectivity of three (Fig. 7b). The topological repeat unit is denoted by degree of vertex (r) and the number of vertices (c) in the topological repeat unit. All the branches are moved to the one side of the chain. The topological repeat unit ${}^cV_r={}^2V_2\ {}^3V_2$ in khurayyimite is half of the size of geometrical repeat unit (Fig. 7c). According to the classification of Day and Hawthorne (2020) the mineral vlasovite $Na_2ZrSi_4O_{11}$ (Sokolova et al. 2006) with chains made of four-membered rings of SiO_4 tetrahedra belongs to the same group (Fig. 7d-f). Another member of the group is synthetic compound $HNb(H_2O)[Si_4O_{11}](H_2O)$ with chains made of six-membered rings.

Supplementary Information The online version contains supplementary material available at https://doi.org/10.1007/s00710-022-00804-z.

Acknowledgements BK acknowledges help from Hannes Krüger, Anuschka Pauluhn and Valerie Goettgens during the synchrotron experiments. The research leading to these results has received funding from the European Union's Horizon 2020 research and innovation program under grant agreement No. 730872, project CALIPSOplus. The field works and microprobe investigations were supported by the National Science Centre (NCN) of Poland, grant 2021/41/B/ST10/00130.

Author contributions EVG, IOG, YV and MM collected the samples in Israel,EVG and IOG performed petrological investigations, microprobe analysis, Raman spectroscopy and optical measurements.BK performed

SC XRD investigation at the synchrotron. BK solved and analyzed the structure.BK and IOG wrote the paper with help from all coauthors.

Funding Open access funding provided by University of Innsbruck and Medical University of Innsbruck.

Declarations

Competing interests The authors declare no competing interests.

References

Abrahams SC, Bernstein JL (1969) Remeasurement of the structure of hexagonal ZnO. Acta Crystallogr B 25:1233–1236

Brown ID, Altermatt D (1985) Bond-valence parameters obtained from a systematic analysis of the Inorganic Crystal Structure Database. Acta Crystallogr B 41:244–247

Burla MC, Caliandro R, Camalli M, Carrozzini B, Cascarano GL, De Caro L, Giacovazzo C, Polidori G, Spagna R (2005) SIR2004: an improved tool for crystal structure determination and refinement. J Appl Crystallogr 38:381–388

Chandra Babu B, Buddhudu S (2014) Analysis of structural and electrical properties of Ni^{2+}:Zn_2SiO_4 ceramic powders by sol–gel method. J Sol-Gel Sci Technol 70:405–415

Day MC, Hawthorne FC (2020) A structure hierarchy for silicate minerals: chain, ribbon, and tube silicates. Mineral Mag 84:165–244

Galuskin EV, Armbruster T, Galuskina IO, Lazic B, Winiarski A, Gazeev VM, Dzierżanowski P, Zadov AE, Pertsev NN, Wrzalik R, Gurbanov AG, Janeczek J (2011) Vorlanite $(CaU^{6+})O_4$ - A new mineral from the Upper Chegem caldera, Kabardino-Balkaria, Northern Caucasus. Russia Am Mineral 96(1):188–196

Galuskin EV, Galuskina IO, Lazic B, Armbruster T, Zadov AE, Krzykawski T, Banasik K, Gazeev VM, Pertsev NN (2011) Rusinovite, $Ca_{10}(Si_2O_7)_3Cl_2$: a new skarn mineral from the Upper Chegem caldera, Kabardino-Balkaria, Northern Caucasus, Russia. Eur J Mineral 23:837–844

Geller YI, Burg A, Halicz L, Kolodny Y (2012) System closure during the combustion metamorphic "Mottled Zone" event. Israel Chem Geol 334:25–36

Hamilton RD, Finney JJ (1985) The structure of junitoite, $CaZn_2Si_2O_7·H_2O$. Mineral Mag 49:91–95

Hogrefe AR, Czank M (1995) Synthetic Dipotassium Zinc Disilicate. Acta Crystallogr C51:1728–1730

Jallad KN, Santhanam M, Cohen MD (2003) Stability and reactivity of thaumasite at different pH levels. Cem Concr Res 33(3):433–437

Kato K, Nukui A (1976) Die Kristallstruktur des monoklinen Tief-Tridymits. Acta Crystallogr B 32:2486–2491

Kesic Z, Lukić I, Zdujić M, Jovalekic C, Liu H, Skala D (2014) Mechanochemical synthesis of $CaO·ZnO·K_2CO_3$ catalyst: Characterization and activity for methanolysis of sunflower oil. Chem Ind Chem Eng Q21:41–41

Khoury HN, Sokol EV, Kokh SN, Seryotkin YV, Nigmatulina EN, Goryainov SV, Belogub EV, Clark ID (2016) Tululite, $Ca_{14}(Fe^{3+}, Al)(Al, Zn, Fe^{3+}, Si, P, Mn, Mg)_{15}O_{36}$: a new Ca zincate-aluminate from combustion metamorphic marbles, central Jordan. Mineral Petrol 110:125–140

Klein H-J, Liebau F (2014) Computerized crystal-chemical classification of silicates and related materials with CRYSTANA and formula notation for classified structures. J Solid State Chem. https://doi.org/10.1016/j.jssc.2008.05.042

Kohara S, Kawahara A (1990) Structure of synthetic dipotassium zinc tetrasilicate. Acta Crystallogr C 46:1373–1376

Li Y, Bass JD (2020) Single Crystal Elastic Properties of Hemimorphite, a Novel Hydrous Silicate. Minerals 10(5):425–434

Liebau F (1985) Structural Chemistry of Silicates: Structure, Bonding, and Classification. Springer-Verlag, Berlin Heidelberg. https://doi.org/10.1007/978-3-642-50076-3

Lin JH, Lu GX, Du J, Su MZ (1999) Phase transition and crystal structures of $BaZn_2Si_2O_7$. J Phys Chem Solids 60(7):975–983

Matschei T, Glasser FP (2015) Thermal stability of thaumasite. Mater Struct 48:2277–2289

Momma K, Izumi F (2011) VESTA3 for three-dimensional visualization of crystal, volumetric and morphology data. J Appl Crystallogr 44:1272–1276

Morimoto N, Nakajima Y, Syono S, Akimoto S, Matsui Y (1975) Crystal structure of pyroxene-type $ZnSiO_3$ and $ZnMgSi_2O_6$. Acta Cryst B31:1041–1049

Novikov I, Vapnik Y, Safonova I (2013) Mud volcano origin of the Mottled Zone, South Levant. Geosci Front 4:597–619

Ntziouni A, Thomson J, Xiarchos I, Li X, Bañares MA, Charitidis C, Portela R, Diz EL (2022) Review of Existing Standards, Guides, and Practices for Raman Spectroscopy. Appl Spectrosc 76(7):747–772

Petříček V, Dušek M, Palatinus L (2014) Crystallographic Computing System JANA2006: General features. Z Für Krist - Cryst Mater 229:345–352

Rentzeperis PJ (1963) The crystal structure of hodgkinsonite $Zn_2Mn[(OH)_2SiO_4]$. Z Für Krist -Cryst Mater 119:117–138

Rigaku (2020) CrysAlisProSoftware System, Version 171.40.53, Rigaku Oxford Diffraction Ltd, Yarnton, Oxfordshire, England

Robinson K, Gibbs GV, Ribbe PH (1971) Quadratic Elongation: A Quantitative Measure of Distortion in Coordination Polyhedra. Science 172:567–570

Rodríguez-Carvajal J (2005) The program Bond_Str and its GUI GBond_Str. Available at: http://mill2.chem.ucl.ac.uk/ccp/web-mirrors/plotr/BondStr/Bond_Str.htm. Last access 14 Nov 2022

Salvadó MA, Pertierra P, García-Granda S, Khainakov SA, García JR, Bortun AI, Clearfield A (2001) Novel Silicate Anion: $Si_8O_{22}^{12-}$. Hydrothermal Synthesis and X-ray Powder Structure of Three New Niobium Silicates. Inorg Chem 40:4368–4373

Sheldrick GM (2008) A short history of SHELX. Acta Crystallogr A 64:112–122

Simonov MA, Sandomirskii PA, Egorov T, Belov NV (1977) The crystal structure of willemite $Zn_2(SiO_4)$. Dokl Akad Nauk SSSR 237:581–588

Sokol EV, Kozmenko OA, Khoury HN, Kokh SN, Novikova SA, Nefedov AA, Sokol IA, Zaikin P (2017) Calcareous sediments of the Muwaqqar Chalk Marl Formation, Jordan: Mineralogical and geochemical evidences for Zn and Cd enrichment. Gondwana Res 46:204–226

Sokolova E, Hawthorne FC, Ball NA, Mitchell RH, Ventura GD (2006) Vlasovite, $Na_2Zr(Si_4O_{11})$, from the Kipawa alkaline Complex, Quebec, Canada: Crystal-Structure refinement and infrared Spectroscopy. Can Mineral 44:1349–1356

Stahl R, Jacobs H (1997) Zur Kristallstruktur von $CaZn_2(OH)_6·2H_2O$. Z Für Anorg Allg Chem 623:1287–1289

Vapnik Y, Galuskin EV, Galuskina IO, Kusz J, Stasiak M, Krzykawski T, Dulski M (2019) Qatranaite, $CaZn_2(OH)_6•2H_2O$: a new mineral from altered pyrometamorphic rocks of the Hatrurim Complex, Daba-Siwaqa. Jordan Eur J Mineral 31(3):575–584

Voronkov AA, Pyatenko YA (1962) The crystal structure of vlasovite. Soviet Physics -Crystallography 6:755–760

Wojdyla JA, Kaminski JW, Panepucci E, Ebner S, Wang X, Gabadinho J, Wang M (2018) DA+ data acquisition and analysis software at the Swiss Light Source macromolecular crystallography beamlines. J Synchrotron Radiat 25:293–303